ChemistrySelect

Research Article
doi.org/10.1002/slct.202404287

Chemistry Europe
European Chemical Societies Publishing

www.chemistryselect.org

Advancing SilverSil Sol–Gel Chemistry Toward Practical Application

Giovanna Li Petri,[a] Rosaria Ciriminna,*[a] and Mario Pagliaro*[a]

Consisting of organically-modified silica entrapping silver nanoparticles originally derived from methyltriethoxysilane (MTES) and tetraethylorthosilicate (TEOS) only, the SilverSil sol–gel coating shows significant antimicrobial activity (in vitro). Now, we report the outcomes of investigation aimed at developing SilverSil coatings to functionalize textiles. We investigate the use of 3-(aminopropyl)trimethoxysilane (APTMS) to stabilize the SilverSil nanosol precursor and increase the Ag nanoparticle encapsulation efficiency. We further study the effect of selected parameters of the sol–gel polycondensation process in sight of practical application of SilverSil as a low-cost antibacterial coating of broad scope and limited antimicrobial resistance.

1. Introduction

Consisting of organically-modified silica (ORMOSIL) entrapping silver nanoparticles (NPs) originally derived from methyltriethoxysilane (MTES) and tetraethylorthosilicate (TEOS), SilverSil is a broad scope antibacterial sol–gel material whose antimicrobial activity so far demonstrated in vitro was first reported in 2020.[1] Colloidal silver (i.e., silver NPs) is a powerful antimicrobial of low toxicity whose mechanism of action minimizes antimicrobial resistance.[2] Accordingly, it comprises the active pharmaceutical ingredient of numerous antimicrobial commercial products widely used across the world since more than a century. Along with Albo, we have suggested that antimicrobial formulations based on microencapsulated Ag NPs will be amid next-generation antimicrobials.[3]

The sol–gel entrapment of metal nanoparticles in ORMOSIL matrices is particularly advantageous due to the pronounced chemical and physical stabilization of the entrapped nanoparticles; the lack of toxicity of the hybrid (organic–inorganic) organosilica coating; and the unique versatility of the sol–gel process that allows to obtain the sol–gel doped material in virtually any shape (powder, film, thin coating, monolith etc.).[4] When applied to kill harmful bacteria, Ag NPs penetrate the bacterial membrane and accumulate therein. Bacteria killed then act as reservoirs of bactericidal Ag NPs that are readily transferred to other bacteria, propagating the bactericidal effect.[5] This is particularly relevant in sight of practical applications of the SilverSil coating, because the hydrophilic–lipophilic balance of ORMOSIL can be widely tuned thanks to the unique versatility of silicon alkoxide chemistry,[6] making these materials ideally suitable for drug release.[7]

In this study we report the outcomes of sol–gel material chemistry research applied to the SilverSil class of materials in view of practical applications aimed at developing practically useful SilverSil coatings. Along with that of MTES, we investigate the use of 3-(aminopropyl)trimethoxysilane (APTMS) as SilverSil co-precursor. In 2011, indeed, Chen and co-workers reported the excellent antibacterial performance of an ORMOSIL derived from TEOS and 3-(2-aminoethylaminopropyl)trimethoxysilane subsequently impregnated with Ag NPs.[8] Furthermore, we investigate the effect of selected parameters including the alkoxide/water ratio, the absence of ethanol as a co-solvent, the time of gel aging, and the alcogel/hydrogel drying conditions.

Findings will be useful to prepare optimized SilverSil coatings to functionalize textile fibers,[9] with which to produce garments with prolonged antibacterial activity, capable to resist prolonged washing cycles.

2. Experimental Section

2.1. Reagents

TEOS (purity grade>99%), MTES (purity grade>99%), APTMS (>99% pure), $NaBH_4$ (purity grade 96%), aqueous nitric acid (65 wt%, purity grade>99%), aqueous ammonia (25 wt%), and $AgNO_3$ (>99.9% pure) were purchased from Sigma–Aldrich (St. Louis, MI, USA). All chemicals were of high purity and were used without any further purification. MilliQ water (Barnstead Smart2Pure Water Purification System, Thermo Scientific) was used in all the sol–gel material syntheses.

2.2. SilverSil and Blank ORMOSIL Preparation

Doped SilverSil materials and their related blank (30% TEOS and 70% MTES, in molar terms, Table 1) were obtained by the sol–gel method (Scheme 1a,b). In particular, three sets of materials were prepared based on different gelation steps (Table 1): set A, including BlankA SilverSilA1,A2,A3 prepared according to the protocol reported previously.[1] BlankB and SilverSilB1, belonging to set B, were obtained by: i) suspending the alkoxide precursors in water instead of ethanol, ii) removing EtOH from alkoxide hydrolysis

[a] Dr. G. Li Petri, Dr. R. Ciriminna, Dr. M. Pagliaro
Istituto per lo Studio dei Materiali Nanostrutturati, CNR via U. La Malfa 153, Palermo 90146, Italy
E-mail: rosaria.ciriminna@cnr.it
mario.pagliaro@cnr.it

Table 1. Blank ORMOSIL and SilverSil samples by gel drying, total alkoxide/EtOH and total alkoxide/H_2O molar ratio.

Sample	Ag (%)	Gel treatment	Total alkoxide/EtOH	Total alkoxide/H_2O
Set A				
BlankA	0.0	Dried at RT for 30 days	0.14	0.05
SilverSilA1	0.01	Dried at RT for 30 days	0.14	0.05
SilverSilA2	0.05	Dried at RT for 30 days	0.14	0.05
SilverSilA3	0.1	Dried at RT for 30 days	0.14	0.05
Set B				
BlankB	0.0	Dried at RT for 30 days	0	0.024
SilverSilB1	0.1	Dried at RT for 30 days	0	0.024
Set C				
BlankC	0.0	Aging 48h, dry at 70 °C	0	0.024
SilverSilC1	0.01	Aging 48h, dry at 70 °C	0	0.024
SilverSilC2	0.05	Aging 48h, dry at 70 °C	0	0.024
SilverSilC3	0.1	Aging 48h, dry at 70 °C	0	0.024
SilverSilC4	1	Aging 48h, dry at 70 °C	0	0.024

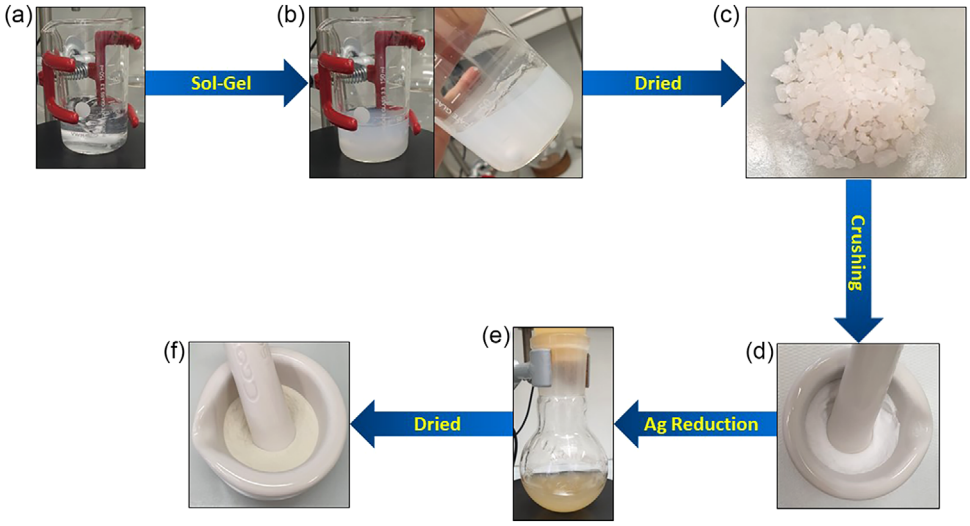

Scheme 1. General workflow of sol–gel preparation of SilverSil xerogel. a,b) Sol–gel transition. c) glassy-looking SilverSil after gel drying. d) Crushed SilverSil powder before reduction of Ag^+. e) Reduction of Ag^+ ions into Ag NPs. f) SilverSil powder doped with Ag NPs.

before the gelation step, and iii) drying the gel at room temperature (RT). Finally, set C (including BlankC and SilverSilC1,C2,C3, and C4 was prepared with the same procedure as set B, but drying the gel in the oven at 70 °C.

In general, aqueous HNO_3 was added to the alkoxide precursors in ethanol, or suspended in water, to catalyze the hydrolysis. After removal of ethanol used as a solvent or derived from hydrolysis, a solution of $AgNO_3$ was added only in the case of SilverSil doped samples (a in Scheme 1). A transparent and colorless gel was then obtained by adding ammonia bringing the pH to 8. Gelation occurred rapidly (Scheme 1b). The wet gel was then left to dry at RT or in the oven (3 days). The xerogel monoliths obtained were crushed into powder in a mortar with a pestle. The blank material was extensively washed with water and then with a 50% (v/v) EtOH: H_2O solution, dried and sieved through the mesh of a laboratory sieve (aperture 150 µm, Cisa Sieving Technologies, Barcelona, Spain). In the case of SilverSil doped preparation the resulting SilverSil xerogel was treated with an excess of $NaBH_4$ solution (1:100) (photo e in Scheme 1). The white suspension turned yellowish or brownish depending on the amount of $AgNO_3$ loaded. The material was filtered through a glass microfiber filters (Whatman, Grade GF/B) and washed first with water, followed by washing with a 50% (v/v) EtOH: H_2O solution, dried in an oven at 40 °C, and finally sieved through a laboratory sieve with a 150 µm aperture (not shown). Photograph f in Scheme 1 shows the SilverSil in final form after the reduction of Ag ions.

Figure 1 displays the blank ORMOSIL next to SilverSil xerogels of increasing Ag load belonging to Set C.

As mentioned above, three sets of materials were prepared (Set A, B, and C). Set A materials (BlankA and SilverSilA1,A2,A3) were prepared as follows: a solution of TEOS (3.94 mL, 17.8 mmol) and MTES (7.85 mL, 39.4 mmol) in 13.3 mL of absolute ethanol, was added with 6 mL of HNO_3 0.2 M dropwise under vigorous stirring at RT, followed after 10 min by APTMS (0.125 mL, 0.716 mmol). For the doped samples SilverSilA1,A2,A3, an aliquot of $AgNO_3$ 6.36 mM (0.5 mL for SilverSilA1, 2.5 mL for SilverSilA2, and 5 mL for SilverSilA3) was slowly added under stirring, followed by addition of ultrapure water to achieve the ratio reported in the Table 1. Gelling was

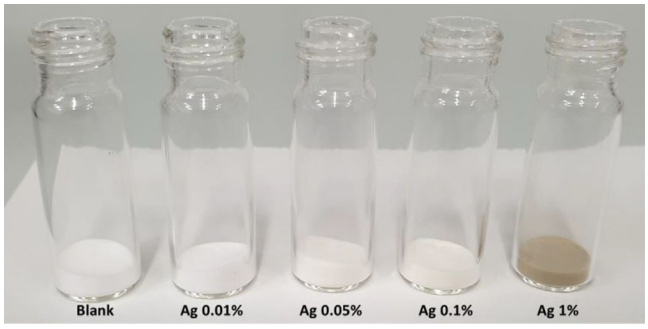

Figure 1. Photographs of blank ORMOSIL and SilverSil samples doped with increasing Ag loadings.

carried out by adding 6 mL of aqueous ammonia 0.2 M dropwise under stirring. The wet gel was dried at RT for 30 days. A sample (1 g) of SilverSil precursor was suspended in 10 mL ultrapure water and stirred with a diluted solution of $NaBH_4$ 0.03 M (0.318, 1.59 and 3.18 mmol, for SilverSilA1,A2, and A3, respectively) for 1 h at RT. Hence, the suspension was filtered and the filtrate washed with 500 mL of water, followed by 200 mL of 50% (v/v) EtOH: H_2O solution, and finally dried in an oven at 40 °C for approximately 5 h.

Set B materials (BlankB and SilverSilB1) were prepared as follows: a mixture of TEOS (3.94 mL, 17.8 mmol) and MTES (7.85 mL, 39.4 mmol) in 13.3 mL ultrapure water, was added with 6 mL of HNO_3 0.2 M dropwise under vigorous stirring at RT. After 10 min, the mixture turned into a solution. The latter solution was added with APTMS (0.125 mL, 0.716 mmol) and left under stirring for 1 h at RT. Ethanol released via alkoxide hydrolysis was removed under reduced pressure (125 mbar) by monitoring the weight loss corresponding to the total amount of ethanol released, and finally, replaced with the same volume (11 mL) of ultrapure water, namely doubling the molar ratio water: alkoxide to prevent rapid polycondensation during the gelation step. In the case of SilverSilB1 an aliquot of 5 mL of $AgNO_3$ 6.36 mM was slowly added, followed by 5 mL of ultrapure water. For the blank material, the aliquot of $AgNO_3$ was replaced with water (5 mL), followed by the aliquot of water to achieve the molar ratio in Table 1. Gelation occurred by adding 3 mL of aqueous ammonia (0.2 M) dropwise. The gel was dried at RT for 30 days. In the case of SilverSilB1, a 1 g sample of the SilverSil precursor material doped with $AgNO_3$ was suspended in 10 mL ultrapure water. The dispersion was added with a dilute solution of $NaBH_4$ 0.03 M (3.18 mmol) and left under stirring for 1 h at RT. The xerogel suspension was filtered and the filtrate washed with 500 mL of water, followed by 200 mL of 50% (v/v) EtOH: H_2O solution. The xerogel was eventually dried in an oven at 40 °C for approximately 5 h.

Set C materials (BlankC and SilverSilC1,C2,C3,C4) were prepared as follows: a dispersion of TEOS (3.94 mL, 17.8 mmol) and MTES (7.85 mL, 39.4 mmol) in 13.3 mL of ultrapure water was added with 6 mL of HNO_3 0.2 M dropwise under vigorous stirring at RT. After 10 min, the dispersion turned into a solution and APTMS (0.125 mL, 0.716 mmol) was added leaving the solution under stirring for 1 h at RT. EtOH originating from the hydrolysis of alkoxides was removed under reduced pressure (125 mbar) and replaced with the same volume (11 mL) of water. In the case of SilverSilC1,C2,C3, an aliquot of $AgNO_3$ 6.36 mM (0.5 mL for SilverSilC1, 2.5 mL for SilverSilC2, and 5 mL for SilverSilC3) was added dropwise, followed by the aliquot of ultrapure water to achieve the ratio reported in Table 1.

In the case of SilverSilC4, a portion (7.95 mL) of a solution $AgNO_3$ 40 mM was added, followed by an aliquot of ultrapure water (2.05 mL) in order to keep the same alkoxide/water ratio. In the case of the blank material, the aliquot of $AgNO_3$ was replaced with water. Gelation occurred by adding 3 mL of aqueous ammonia 0.2 M dropwise. The wet hydrogel was aged for 48 h at RT and then dried in an oven at 70 °C for 3 days. A 1 g sample of the SilverSil xerogel precursor doped with $AgNO_3$ was suspended in 10 mL ultrapure water (in 20 mL, in the case of SilverSilC4) and added under stirring with a solution of $NaBH_4$ 0.03 M (0.318, 1.59, 3.18, and 31.8 mmol for SilverSilC1,C2,C3,C4, respectively) for 1 h a RT. Finally, the suspension was filtered and washed with 500 mL of water, followed by 200 mL of 50% (v/v) EtOH: H_2O solution. The washed xerogel was dried in an oven at 40 °C for approximately 5 h.

2.3. Materials Characterization

The FTIR spectra were recorded with a Fourier-transform infrared spectrophotometer (Bruker, Billerica, MA, USA) in the range 400 – 4000 cm^{-1}, with lateral resolution of 4 cm^{-1} and 128 scans per sample. All material powders were mixed with ultrapure KBr (FTIR grade, ≥99% pure, Sigma–Aldrich) at weight ratio (mg) of 100:1, using a pestle and mortar. The finely obtained mixture was molded into a disc shape using a Specac Mini-Pellet laboratory hydraulic press applying a 12-t weight. X-ray diffraction (XRD) patterns were obtained using a D5005 X-ray diffractometer (Bruker AXS, Karlsruhe, Germany) operating at 40 kV and 30 mA. The diffraction profile was obtained at a 0.15°/min acquisition rate, spanning a 10.0°– 80.0° 2θ range. The X-ray radiation, generated through a copper (K–α) anode, was rendered monochromatic via the instrument's secondary monochromator. The ζ-Potential of material suspension (material sifted through a 150 µm mesh sieve) in ultrapure water (5 mg/mL) kept at pH of 7.4 was measured in a folded capillary cell (Malvern Zetasizer Nano Series) using a Malvern Zetasizer Nano ZS (Malvern Panalytical, Malvern, Great Britain) equipped with a He–Ne laser at a power of 4.0 mW operating at a wavelength of 633 nm. The field emission scanning microscope (FE–SEM) photographs were taken with a Zeiss LEO 1530 (Carl Zeiss NTS, Oberkochen, Germany) with an accelerating voltage of 20 kV. The thermogravimetric analysis (TGA) was conducted using a Mettler Toledo TGA/DSC. Each time, a sample weighing approximately 15 mg kept under nitrogen was heated from room temperature to about 800 °C at 10 °C/min rate.

The specific surface area (SSA), specific pore volume (SPV), and pore size distribution were assessed from the adsorption–desorption isotherms of cryogenic N_2 as adsorbate using the Quantachrome (Boynton Beach, FL, USA) NOVA 2000e material analyzer. Prior to analysis, the sample underwent degassing under vacuum at 200 °C for 120 min. The SSA was determined utilizing the multipoint Brunauer–Emmett–Teller (BET) model, employing the average adsorption and desorption values of relative pressure P/P_o within the range of 0–0.98 at the fixed temperature of 77.4 K. The pore size distribution and SPV were calculated by applying the Barrett–Joyner–Halenda (BJH) model to the desorption branch of the isotherms across the whole P/P_o range. Experimental data were processed using the OriginPro software, version 2024 (OriginLab, Northampton, MA, USA).

3. Results and Discussion

The FTIR spectra of blank and SilverSil materials doped with Ag^+ or with metal nanoparticle Ag^0 in Figure 2 shows the typical silica fingerprint bands in the 950–1250 cm^{-1} region, namely the ν_{as}Si—O—Si mode, split in two observable components, with maxima at ~1130 and ~1050 cm^{-1} corresponding to the longitudinal and transverse optical components (LO and TO, respectively) of different siloxane rings: six-member $[(SiO)_6]$

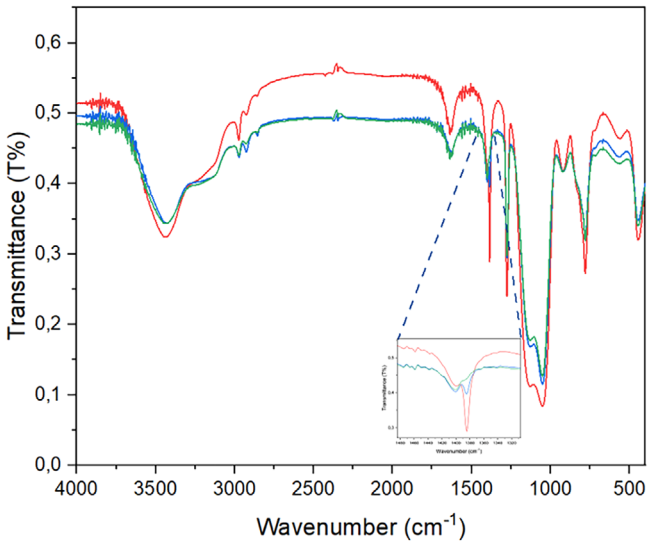

Figure 2. FTIR spectra of BlankC ORMOSIL (blue line), doped SilverSilC3 before (red line), and after (green line) reduction with $NaBH_4$.

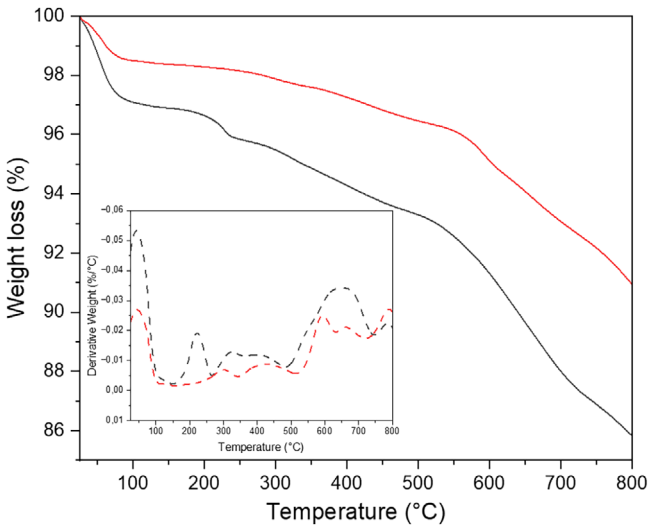

Figure 4. Weight loss percentage (straight line) and derivative curves (dashed lines) of BlankC ORMOSIL (black line) and SilverSilC3 (red line).

and four-member $[(SiO)_4]$.[10] The bands at 920 cm^{-1} and 779 cm^{-1} are, respectively, those of Si—OH stretching, and symmetric v_sSi—O—Si vibration mode.

The broad common band centered at 3438 cm^{-1} is characteristic of O—H stretching vibrations due both to O—H stretching mode of both adsorbed water and silanol groups. The O—H bending signal is visible at around 1640 cm^{-1}.[11] However, this band is superimposed to the N—H stretching vibration of the NH_2 functional group of APTMS, and with that of residual silanol groups (Si—OH) located at the surface of the silica particles. Peaks at 2971 and 2922 cm^{-1} are relative to the stretching vibrations of C—H bonds of aliphatic -CH_2 propyl amino chain, that are overlapped with the antisymmetric and symmetric, respectively, stretching modes of the methyl group bound to the Si atom.[10] The Si-CH_3 group is also recognized by a strong and sharp band at 1270 cm^{-1}.

The SilverSil material (SilverSilC3 before reduction with $NaBH_4$) entrapping the Ag^+ ions not yet reduced to Ag^0 nanoparticles shows a sharp and intense absorption band at 1385 cm^{-1} due to the C—N stretching vibration[12] that is significantly stronger compared to blank material due to the asymmetric N—O stretching in the NO_3^- group,[13] and the increased C—N stretching originating from the interaction of the positive charge of Ag^+ with the electron-pair donors of NH_2 functional groups.[14] This electronic interaction keeps the silver species highly dispersed and may hinder the growth of Ag NPs into large metal clusters during the reduction step. Remarkably, the peak at 1385 cm^{-1} disappears after reduction of Ag^+ ions into metal species. In other words, the strong interaction between the amine group of APTMS and the Ag NPs at the surface of the sol-gel cages dramatically reduces the C—N stretching vibration.

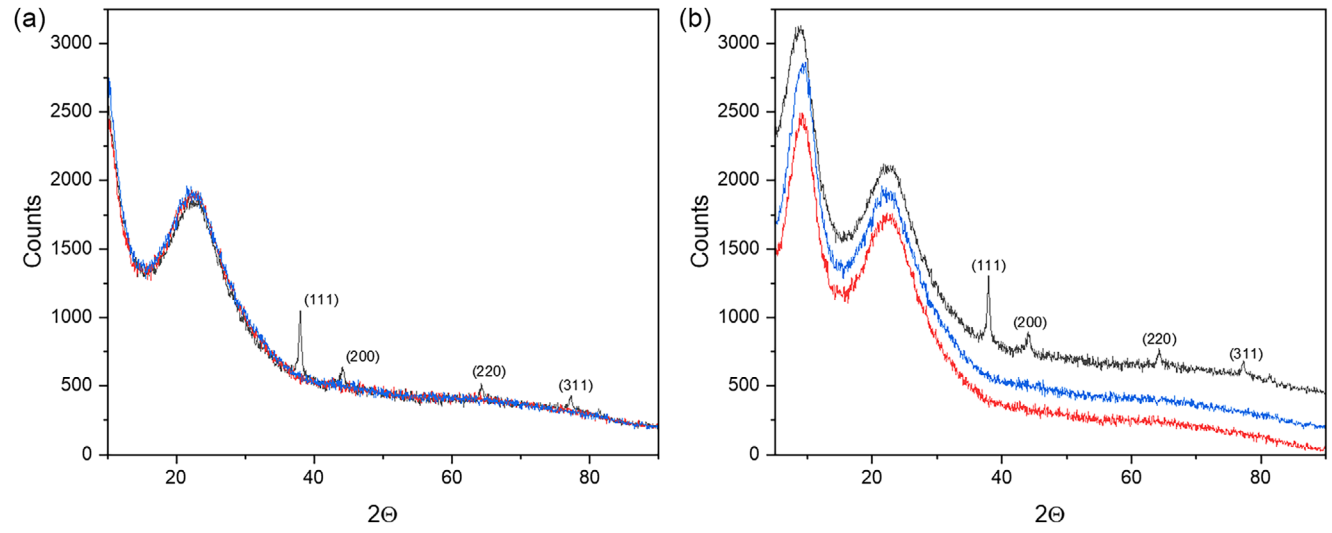

Figure 3. (a) Stacked and (b) unstacked XRD patterns of BlankC ORMOSIL (red curve), SilverSilC3 (blue curve), and SilverSilC4 (black curve).

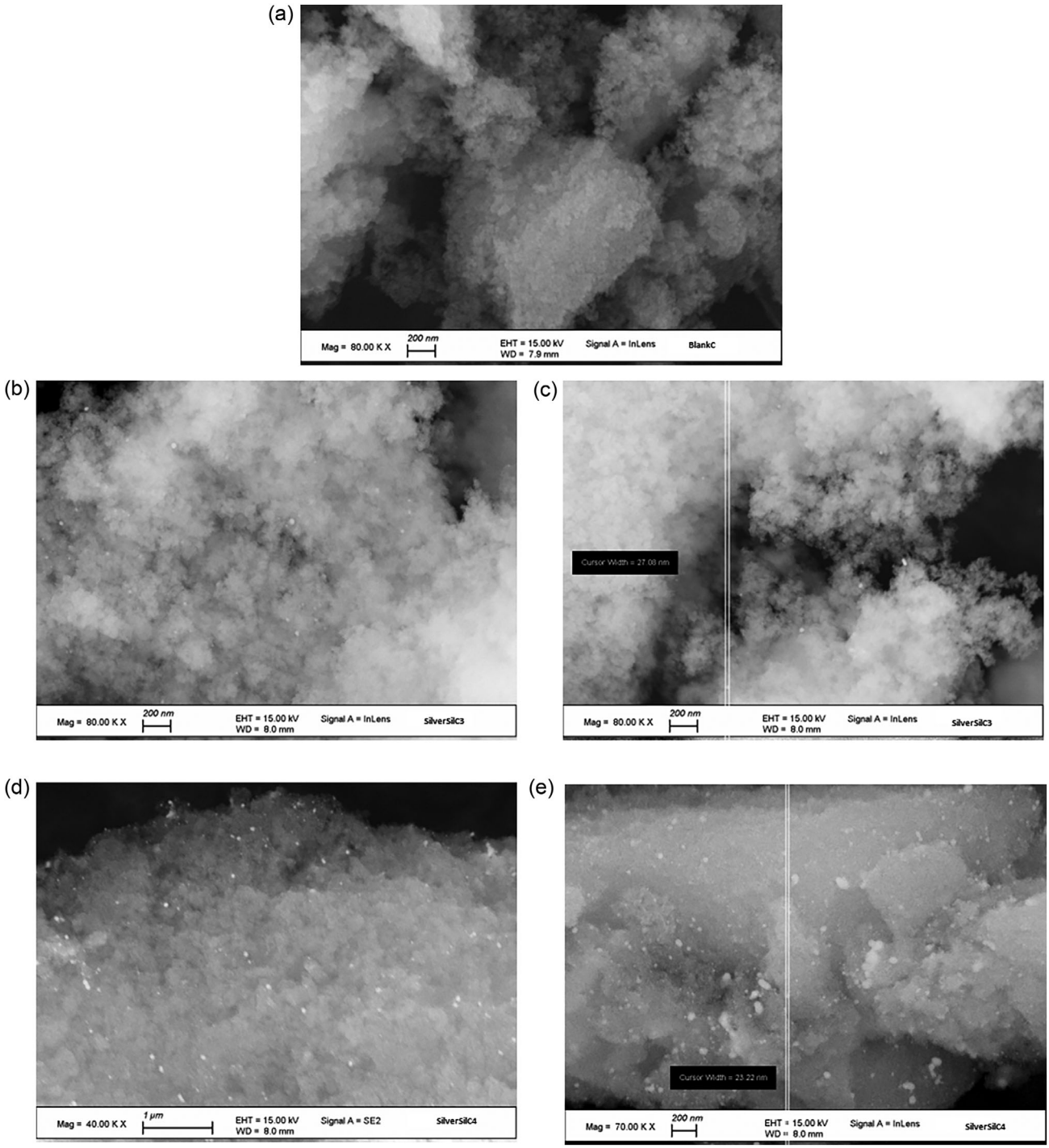

Figure 5. SEM photographs of a) BlankC ORMOSIL, b,c) SilverSilC3, and d,e) SilverSilC4.

The XRD patterns in Figure 3 confirm the well-known amorphous structure of all the ORMOSIL materials: the doped SilverSilC3,C4, and the BlankC ORMOSIL materials. The broad peak centered at $2\theta \approx 23°$ pointing to the Bragg *d*-spacing of 4 Å originates from the constant spacing between silicon atoms in the siloxane Si—O—Si units of the xerogel matrix.[15]

The diffraction peaks of metallic Ag were not observed in SilverSilC3 (0.0318 mmol of $AgNO_3$ used in the preparation) likely due to the low concentration, as reported introducing the SilverSil class of materials.[1] In contrast, the diffraction signals of metallic Ag (peaks at 37.9°, 44.4°, 64.2°, and 77.2° corresponding to the (111), (200), (220), and (311) planes of crystalline Ag)[16] is evident for the SilverSilC4 material in which the amount of $AgNO_3$ used during the material sol–gel synthesis was ten times higher (0.318 mmol).

The TGA/DTG curves of BlankC and doped SilverSilC3 in Figure 4 show a first weight loss up to 100 °C due to water loss for both samples.

Table 2. ζ-potential of SilverSil and blank ORMOSILs.

Material	ζ -potential (mV)
BlankA	27.5 ± 4.78
SilverSilA1	24.9 ± 5.61
SilverSilA2	23.1 ± 5.56
SilverSilA3	22.4 ± 5.43
BlankB	31.6 ± 6.41
SilverSilB1	21.8 ± 4.71
BlankC	24.8 ± 6.29
SilverSilC1	18.6 ± 7.68
SilverSilC2	18 ± 7.37
SilverSilC3	19.8 ± 3.37
SilverSilC4	18.5 ± 4.04

The weight loss between 200 °C and 400 °C is due to the decomposition of aliphatic amine chains. This is consistent with the DTG curves, which suggest that the interaction between Ag and $-NH_2$ in doped sample weakens the scission rate of the aminosilane chain.[17,18] In general, the relatively small weight loss up to 800 °C (about 16% for BlankC and 11% for doped SilverSilC3) suggests that more than 80% of the weight is composed of silica, with or without silver, and thus indirectly that nearly complete hydrolysis of silane precursors occurs during the sol–gel process.

Figure 5 shows they FE–SEM photographs of SilverSilC3,C4, and BlankC ORMOSIL samples.

Clearly visible in the photographs of the doped SilverSil xerogels, the Ag NPs have spherical shape and uniform size dispersion around 20–25 nm in diameter for both SilverSilC3 and SilverSilC4 (Figure 5b–e). In the latter sample, ellipsoidal-shaped particles are occasionally observed (Figure 5d,e), likely due to the higher Ag concentration increasing the likelihood of agglomeration during the reduction of silver ions to metallic Ag atoms and subsequent aggregation into metal clusters and nanoparticles.

The colloidal stability and surface charge of the SilverSil microparticles dispersed in water at neutral pH were assessed through ζ-potential measurement. The analysis clearly revealed a positive charge on the surface of the organosilica microparticles, both in blank ORMOSIL and doped SilverSil materials. Overall, values in Table 2 show evidence that all doped SilverSil materials show lower ζ-potential values, ranging from 18 to 24.9 mV. The silver-free blank samples have higher ζ-potential values, ranging from 24.8 to 31.6 mV, regardless the method of preparation.

This differenceonce again points to the strong interaction of $-NH_2$ groups at the surface of the SilverSil microparticles and the Ag NPs at the surface of the sol–gel cages. The interaction, observed also in previous studies on periodic mesoporous silicas [17] and in aminopropyl-modified silica,[18] reduces the amount of NH_3^+ groups formed in the aqueous phase upon hydrolysis of the $-NH_2$ groups pending the outer surface of the SilverSil material.

Finally, the adsorption/desorption isotherms in Figure 6 show the mesoporous nature of SilverSil materials with pore size less than 20 nm and isotherms of intermediate between type-IV and type-II. The hysteresis loops close to type H1, is characteristic of capillary condensation in open cylindrical mesopores between spheroidal particles of fairly uniform array,[19] large surface area and pore volume. Higher slopes were observed for the adsorption isotherms of BlankC and SilverSilC3 at relative pressure (P/P_o) above 0.9 (Figure 6e,f, respectively). For these materials, drying was conducted in the absence of ethanol (removed under vacuum). On the other hand, BlankB and its doped analogue SilverSilB1 showed intermediate slopes (Figure 6c,d, respectively). This observation suggests that in the absence of EtOH, drying the hydrogel at RT or in an oven drives formation of larger pores[20] (see the pore size trend in Table 3).

In further detail, values in Table 3 show that the blank ORMOSIL BlankA (1062 m^2/g) and its SilverSil doped analogue SilverSilA3 (857 m^2/g) have the highest values of SSA, and type-IV adsorption-desorption isotherms (Figure 6a,b, respectively).

In addition, the higher SSA values for SilverSil samples gelled in the presence of higher amounts of EtOH and dried at room temperature (BlankA and SilverSilA1, A2, and A3) is due to lower capillary forces at the surface of the as-formed sol-cages during evaporation at room temperature of the aqueous EtOH. Prolonged and gradual drying at RT promotes reduced shrinkage of the alcogels compared to drying at 70 °C.

Taken together, these findings are important towards practical application of SilverSil to functionalize fabrics because, as highlighted by Böttcher, whose team in Germany collaborated for nearly 20 years with textile companies towards the industrial uptake of functional sol–gel coatings, all sol–gel coatings based on TEOS and alkoxysilanes contain flammable alcohol, whereas if the alcohol is removed from the coating solution, it becomes unstable and gels quickly.[21]

Using the newly developed alcohol-free SiliverSil coating formulations developed in this work affords both high Ag NP encapsulation efficiency and high nanosol stability against aggregation (see Table 3) due to the significant stabilization effect of the APTMS added at just 1.8 mol% of the amount of MTES employed in the sol–gel polycondensation.

This is important because high dispersion through atom economy approaches wherein much of the silver atoms are present at the outer surface rather than agglomerates in the bulk, highlight the need for such high dispersion of silver for highest antimicrobial activity.[22]

Readily deposited on fabrics forming a lyogel (from the Greek "lyo" for solvent) drying at room temperature,[9] the SilverSil coating will be used to form the homogeneous coating safely imparting textiles with antimicrobial properties. This study established the optimal coating composition and preparation conditions. The outcomes of antimicrobial tests using different fibers will be reported soon.

It is worth mentioning, in conclusion, that a similar approach was followed by Procaccini and co-workers who first demonstrated stabilization and slow release in water of Ag metal clusters in ORMOSIL coatings derived from TEOS

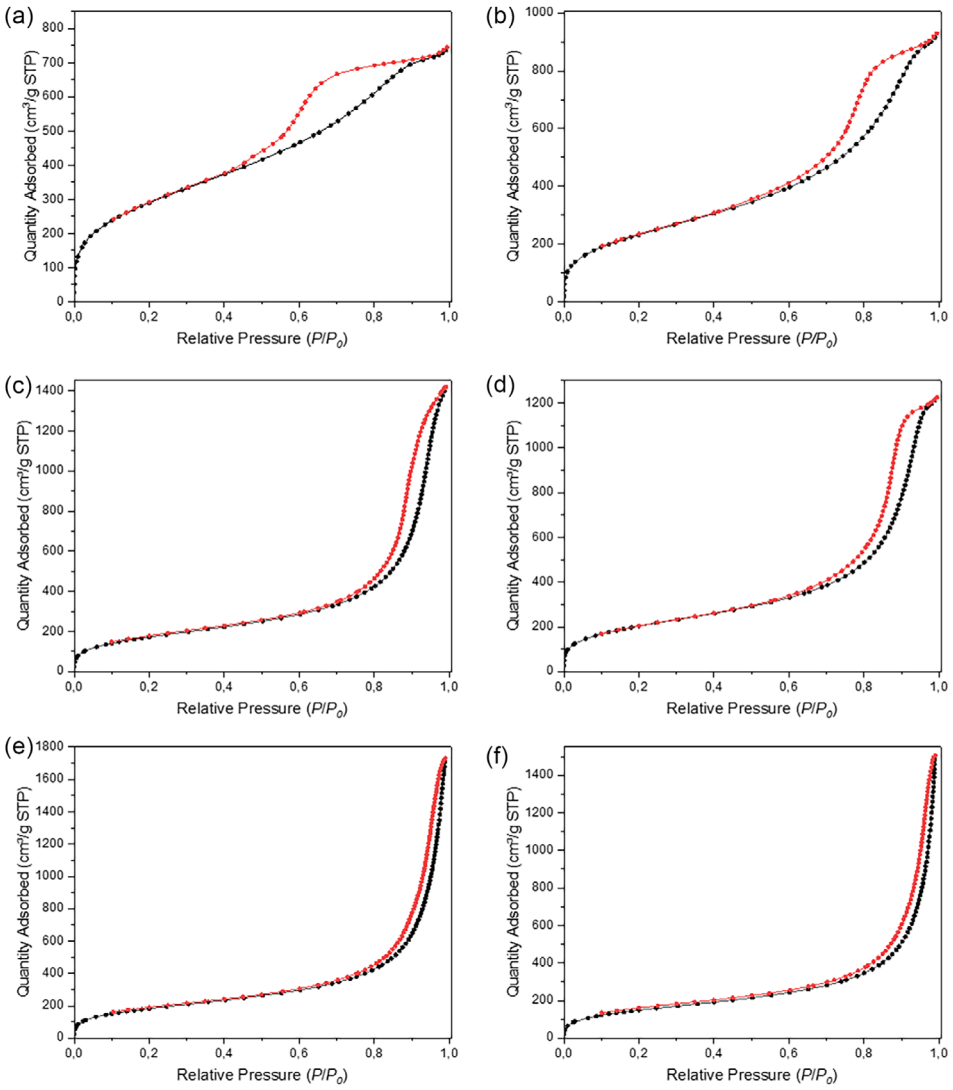

Figure 6. N_2 adsorption (black curve)/desorption (red curve) isotherms of (a) BlankA and (b) SilverSilA3, (c) BlankB and (d) SilverSilB1, (e) BlankC and (f) SilverSilC3.

Table 3. Specific surface area (SSA), pore specific volume (PSV), and pore size of Blank SilverSil materials.

Samples	SSA (m^2/g)	PSV (cm^3/g)	Pore Size (nm)
BlankA	1062	1.10	4.37
SilverSilA1	1088	1.41	5.42
SilverSilA2	748	1.26[a)]	7.44[b)]
SilverSilA3	857	1.48	6.31
BlankB	640	2.17	14.09
SilverSilB1	747	1.86	10.69
BlankC	674	2.63	17.41
SilverSilC3	551	2.29	18.33

[a)] BJH Adsorption cumulative volume of pores;
[b)] BJH Adsorption average pore width.

and MTES,[23] and subsequently demonstrated the antibacterial activity of said coatings deposited on surgical-grade stainless steel.[24]

4. Conclusion

The structural investigation of SilverSil ORMOSIL coatings prepared through a two-step sol–gel hydrolytic polycondensation of TEOS and organically modified silanes MTES and APTMS varying readily controlled parameters of the sol-gel process unveils numerous aspects that will be instrumental towards the first practical application of this promising class of antimicrobial sol–gel coatings.

First, the amine functional group in APTMS acts as a stabilizer for silver atom clusters during reduction, preventing aggregation into larger particles, and stabilizing the colloidal nanosol precursor of the xerogel.

Second, EtOH removal prior to gelation via evaporation under reduced pressure is beneficial because the alcohol may reduce some of the added Ag^+ ions before gelation eventually causing silver loss in the subsequent washing and drying steps.

Third, the gel-drying step substantially influences the Ag NPs encapsulation efficiency. Slow drying, even in the absence of ethanol, translates into lower encapsulation efficiency likely due to migration of Ag^+ to the outer surface of the sol–gel cages of the xerogel, from which some Ag NPs may be lost during the subsequent xerogel washing step.

Acknowledgements

The authors acknowledge funding supporting the work of G.L.P. via the Made in Italy – Circular and Sustainable (MICS) Extended Partnership funded by the European Union NextGenerationEU (PNRR – Missione 4, Componente 2, Investimento 1.3 – D.D. 1551.11–10–2022, PE00000004). The authors thank Dr Gabriella Di Carlo and Dr Cristina Riccucci, Istituto per lo Studio dei Materiali Nanostrutturati, CNR, Montelibretti, for the FE–SEM measurements.

Conflict of Interests

The authors declare no conflict of interest.

Data Availability Statement

The data that support the findings of this study are available from the corresponding authors upon reasonable request.

Keywords: Antibacterial · ORMOSIL · Silver nanoparticle · SilverSil · Sol–gel

[1] K. Trabelsi, R. Ciriminna, Y. Albo, M. Pagliaro, *ChemistryOpen* **2020**, *9*, 459463.
[2] S. Tang, J. Zheng, *Adv. Healthcare Mater.* **2018**, *7*, 1701503.
[3] R. Ciriminna, Y. Albo, M. Pagliaro, *ChemMedChem* **2020**, *15*, 1619–1623.
[4] D. Avnir, *Acc. Chem. Res.* **1995**, *28*, 328–334.
[5] R. K. Wakshlak, R. Pedahzur, D. Avnir, *Sci. Rep.* **2015**, *5*, 9555.
[6] I. Roy, P. Kumar, R. Kumar, T. Y. Ohulchanskyy, K.-T. Yong, P. N. Prasad, *RSC Adv.* **2014**, *4*, 53498–53504.
[7] A. Fidalgo, R. Ciriminna, L. M. Ilharco, M. Pagliaro, *Chem. Mater.* **2005**, *17*, 6686–6694.
[8] K. H. Wu, C. I. Liu, C. C. Yang, G. P. Wang, C. M. Chao, *Mater. Chem. Phys.* **2011**, *125*, 802–806.
[9] R. Ciriminna, Y. Albo, M. Pagliaro, *ChemistrySelect* **2020**, *5*, 9776–9780.
[10] A. Fidalgo, R. Ciriminna, L. Lopes, V. Pandarus, F. Béland, L. M. Ilharco, M. Pagliaro, *Chem. Centr. J.* **2013**, *7*, 161.
[11] S. Duhan, N. Kishore, P. Aghamkar, S. Devi, *J. Alloys Compd.* **2010**, *507*, 101–104.
[12] S. Y. Lin, S. T. Chang, *J. Phys. Chem. Solids* **1998**, *59*, 1399–1405.
[13] N.B. Kondrashova, A. S. Shamsutdinov, V. A. Valtsifer, *J. Inorg. Organomet. Polym.* **2021**, *31*, 1347–1358.
[14] A. Tăbăcaru, C. Pettinari, M. Bușilă, R. M. Dinică, *Polymers* **2019**, *11*, 1686.
[15] S. L. B. Lana, A. B. Seddon, *J. Sol–Gel Sci. Technol.* **1998**, *13*, 461–466.
[16] T. Thirugnanasambandan, M. Alagar, *Nano Biomed. Eng.* **2012**, *4*, 58–65.
[17] P. Taba, P. Budi, A. A. Gau, Y. Hala, St. Fauziah, I. W. Sutapa, J. Manga, *Rasayan J. Chem.* **2021**, *14*, 204–211.
[18] G. Pavoski, D. L. Stamm Baldisserotto, T. Maraschin, L. F. Wentz Brum, C. dos Santos, J. H. Zimnoch dos Santos, A. Brandelli, G. Barrera Galland, *Eur. Polymer J.* **2019**, *117*, 38–54.
[19] S. J. Gregg, K. S. W. Sing, *Adsorption, Surface Area, and Porosity*, Academic Press, New York **1982**.
[20] Q. Chen, Y. Ge, H. Granbohm, S.-P. Hannula, *Nanomaterials* **2018**, *8*, 362.
[21] B. Mahltig, H. Haufe, H. Böttcher, *J. Mater. Chem.* **2005**, *15*, 4385-4398.
[22] H. Mude, P. Tata, T. Jamma, R. Ganesan, J. Ray Dutta, *Adv. Therap.* **2023**, *6*, 2300015.
[23] R. Procaccini, S. Ceré, S. Pellice, *Surf. Coat. Tech.* **2011**, *205*, 5464–5469.
[24] R. Procaccini, A. Bouchet, J.I. Pastore, C. Studdert, S. Ceré, S. Pellice, *Prog. Org. Coat.* **2016**, *97*, 28–36.

Manuscript received: September 7, 2024